ELSEVIER

Catalysis Today 50 (1999) 661–668

CATALYSIS TODAY

Predicting locations of non-framework species in zeolite materials

V.V. Guliants[a,*], J.T. Mullhaupt[a], J.M. Newsam[b], A.M. Gorman[b], C.M. Freeman[b]

[a]*Praxair Inc., 175 East Park Drive, PO Box 44, Tonawanda, NY 14151, USA*
[b]*Molecular Simulations Inc., 9685 Scranton Road, San Diego, CA 92121, USA*

Abstract

A new grid-based algorithm developed at Molecular Simulations, and molecular dynamics method have been applied to modeling the locations of non-framework species in zeolites. This new method locates the energy minima for various frameworks and populates these sites with the non-framework species. The cation locations were predicted in dehydrated zeolite adsorbents and catalysts, such as $Na_{88}X$, $Ca_{48}X$, mixed cation zeolite 3A ($K_{60}Na_{36}A$), and Cu-mordenite (Si/Al=5.0) using only well-known framework structure models. Furthermore, the locations of benzene molecules in a supercage of zeolite $Ca_{48}X$ were correctly predicted via the application of the Monte Carlo docking and molecular dynamics methods.

These examples demonstrate that when the framework type is known, the new technique can provide a realistic initial structure input for the challenging task of solving crystal structures of zeolites containing non-framework species.

Keywords: Zeolite; Molecular dynamics; Non-framework species

1. Introduction

The nature and location of the non-framework species define ion-exchange, sorptive and catalytic properties of zeolites and molecular sieves. The experimental location of non-framework species by diffraction techniques is complicated by the polycrystalline nature of the zeolite phases and often low symmetry and occupancy of non-framework crystallographic sites [1,2]. Molecular modeling methods are becoming increasingly useful as an aide to the interpretation of experimental data, especially when only a fraction of the non-framework species can be located in the experiment. Previous approaches employed simple site-filling or statistical thermodynamical models to obtain relative site energies in various cation-exchanged forms of the cubic [3–8] and hexagonal faujasites [9] and zeolite ZK-5 [10], as well as estimation of short- and long-range interactions in controlling site occupancy patterns [11]. Recently developed combined Monte Carlo packing/structure optimization technique located non-framework cations based solely on the knowledge of the framework structure. This method was relatively quick, and produced encouraging results for simple systems. However, for more complex systems, more sophisticated simulation strategies were needed, such as simulated annealing techniques [12,13].

We describe here the application of a new modeling method to several zeolite adsorbent and catalyst systems for which reasonable structural data are available. Similar to the combined Monte Carlo/structure optimization method [12,13], the new technique gen-

*Corresponding author. Tel: +1-716-879-7006; fax: +716-879-7030; e-mail: vadim_guliants@praxair.com

0920-5861/99/$ – see front matter
PII: S0920-5861(98)00500-8

erated non-framework cation positions using only the zeolite framework information. The new method was applied to more complex systems of the current study, such as NaX and mixed cation zeolite 3A. Moreover, it provided realistic structural models that can be used to solve crystal structures of zeolites containing non-framework species.

2. Simulation methodology

2.1. Zeolite frameworks

To model zeolites $Na_{88}X$ (Si/Al=1.18) and $Ca_{48}X$ (Si/Al=1.0), which contain a single type of non-framework species, structural model of the zeolite X framework was first generated using the experimental data of Olson [14]. For $Na_{88}X$, eight aluminum sites per unit cell were randomly substituted by silicon to give a Si/Al ratio of 1.18. In the case of zeolite A (LTA) framework (Si/Al=1.0), the experimental data of Gramlich and Meier [15] were used. For Cu-mordenite, two scenarios were modeled. First, the all-silica mordenite (MOR) framework possessing the $Cmc2_1$ space group symmetry [16] was used in the simulation due to the uncertainty in the Al atom distribution in the framework. The Si atom charge was reduced accordingly to reproduce the negative framework charge (−8.0) in the *P1* unit cell ($Si_{48}O_{96}$) corresponding to that in the naturally occurring mordenite (Si/Al=5.0). In the second case, a random distribution of the eight Al atoms in the Si/Al=5.0 mordenite framework was assumed.

2.2. Location of non-framework species

The detailed description of the new grid-based technique may be found elsewhere [17,18]. Charges and van der Waals parameters were assigned to each framework atom in accordance with the augmented *cvff_aug* forcefield validated for aluminosilicates [19]. The cations in this forcefield bore formal charges, while the framework atoms had the following charges: O=−1.2, Si=+2.4, and Al=+1.4. A three-dimensional *host reference grid* with grid spacing of ca. 0.5 Å was created commensurate with the framework symmetry and unit cell size. Since the generated grid is commensurate with the symmetry of the host, a symmetry operator will exactly map one grid point onto another. The cation-framework non-bonding electrostatic and a repulsive–dispersive interactions were calculated at each grid point using the Ewald summation method and a short range 5.5 Å cutoff, respectively. Since a charged periodic structure was used in the calculation, the electroneutrality of the periodic cell was achieved by adding a homogeneous background term to the reciprocal space contribution to the Ewald sum [18]. For computational efficiency, only symmetry-unique grid points needed to be calculated, and the values mapped onto their symmetry equivalents [17]. A second, so-called *cation reference grid* of identical dimensions were constructed, a single cation placed at its origin, and the interaction of a second cation at each grid point was computed. A cation was placed in the framework at the lowest energy position found in the preceding step, i.e. during computation of the cation-framework interaction. Since the framework contained an additional cation, the reference grid was updated by superimposing it with the cation reference grid, centered about the location of the recently added cation. The lowest energy position was again determined and populated. These steps were repeated until all cations were added to the X framework. In the case of zeolite 3A, containing both K^+ and Na^+ cations, Na^+ cations were added first, since they were expected to occupy the sites of lowest energy associated with the bare framework due to higher z/r ratio.

2.3. Lattice energy minimization

The crude cation locations found in the preceding step were optimized using molecular mechanics *Discover 3.2* energy minimization engine [20], with the framework initially held rigid. The entire extent of the unit cell was then allowed to relax. In all the partial and full-structure optimizations, the unit cell parameters were held fixed which corresponded to constant volume minimization. In these calculations, the equilibrium structures were constrained to the crystallographic volume. The potential energy function describing the non-bonded pairwise interactions between ions included Columbic and short-range Lennard-Jones 12–6 potential:

$$V(r_{ij}) = \frac{q_i q_j}{r_{ij}} + \frac{A_{ij}}{r_{ij}^{12}} - \frac{B_{ij}}{r_{ij}^{6}},$$

where q_i and q_j are the charges of the interacting ions i and j, and A_{ij} and B_{ij} are short-range repulsion and dispersion parameters, respectively.

In the case of the benzene/$Ca_{48}X$ system, high temperature molecular dynamics was performed on benzene molecule in the gas phase to produce a library of its conformations, followed by a series of random insertions of benzene into the $Ca_{48}X$ model using a *Solids_Docking* Monte Carlo procedure of *Catalysis* [21]. The locations of crudely docked benzene molecules were then optimized at constant volume to yield representative low energy binding sites for the flexible benzene molecules within the host structure [20].

3. Results and discussion

3.1. NaX

Olson [22] found three Na^+ non-framework sites: sites I′, II and III in the structure of $Na_{88}X$ in a recent single crystal XRD study. These and other common non-framework sites found in faujasites are shown in Fig. 1.

Site I is located at the center of a hexagonal prism, or a double 6-ring (D6R) connecting sodalite or β-cages. This cation site offers a favorable octahedral coordination environment and is occupied in NaY structure. Site I′ are situated in the hexagonal prisms in the plane of the 6-ring. Low symmetry sites III and III′ are located directly above and on the edges of the

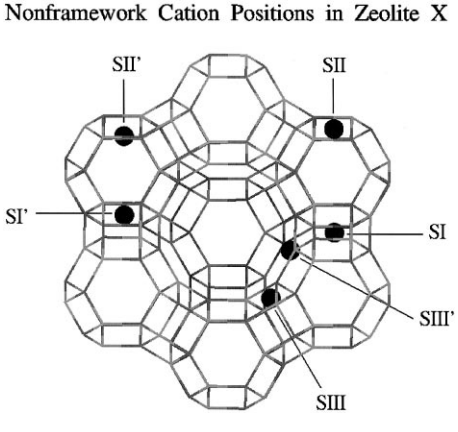

Fig. 1. Non-framework cation positions in zeolite X.

4-rings (4R) in the supercage, respectively. According to Olson [22], Na^+ cations (29.1/u.c.) in site I′ in NaX (Si/Al=1.18) were split between two closely related positions in proportion to the number of 6-rings containing three and two Al atoms [22]. In addition to Na^+ cations in site I′, Olson [22] found 2.9 Na^+/u.c. in site I. Cheetham et al. [1] found site I′ fully occupied by Na^+ cations in a powder neutron diffraction study conducted at 5 K. In both structure studies site II were found to be fully occupied [1,22].

In contrast to crystallographic sites I and II, cations in non-framework sites III and III′ are very difficult to locate experimentally due to their low symmetry and occupancy. Earlier, Smolin et al. [23] located only 9.9 out of 31.4 Na^+ cations in the unit cell of $Na_{92}X$ in a single crystal XRD study. Olson [22] found the remaining 29.8 Na^+ cations in three crystallographically distinct site III′ located above the edges of the 4-rings tricoordinated to oxygen atoms. Na–O distances in these sites range from short (2.22 Å) to much longer (3.61 Å) than the idealized sum of ionic radii. Na5 ions in site III′ are located 2.22 Å above the O4 oxygen atoms of the 4-rings and 2.83 Å away from the two O1 oxygens [22]. Na6 ions are displaced toward hexagonal prism oxygens, having a Na6–O4 distance of 2.58 Å and two Na6–O1 distances of 2.45 and 3.61 Å [22]. Na6′ cations are also displaced toward hexagonal prism oxygens: Na6′–O4=2.22 Å, Na6′–O1=2.44 and 3.39 Å [22]. Cheetham et al. [1] found only one low symmetry site for the remaining 24 Na^+ cations in the supercage. Na^+ cations in their site III′ are located in the vicinity of the Na6 site of Olson [22] facing (AlO_4) tetrahedra. In fact, the site III′ location found by Cheetham et al. [1] is only 0.20 Å apart from the Na6 site of Olson.

We attempted to locate Na^+ sites in the supercages of zeolite X, since the general agreement exists regarding Na^+ locations in high symmetry crystallographic sites I and II [1,22,23]. In this study, Na^+ cations were placed in sites I′ and II to achieve their full occupancy [1] and held rigid during subsequent procedure to locate the remaining 24 cations. The present method located 18 Na^+ cations within 0.16–0.35 Å of site III′ [1] in the supercage (Fig. 2). These cations were coordinated to two oxygen atoms, O1 and O4, at a distance of 2.38 Å, facing (AlO_4) tetrahedra (Fig. 2). This Na^+ location is in agreement with the experimental and modeling data of Cheetham et al. [1]. Na^+

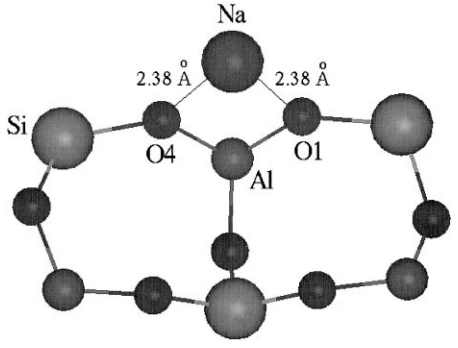

Fig. 2. Predicted location of Na^+ cations in Site III′ of zeolite X.

cations positioned in the vicinity of the (AlO_4) tetrahedra compensate locally the negative charge on the framework. The remaining six Na^+ cations were located near Na6′ site III′ of Olson [22] where they face (SiO_4) tetrahedra. For comparison, the locations of all Na^+ cations in the unit cell were also modeled. For computational expediency, we modeled a primitive unit cell of NaX ($Na_{22}Al_{22}Si_{26}O_{92}$), which is four times smaller than the full unit cell. The cation location pattern in the primitive unit cell of NaX was 8 (I+I′), 8 (II) and 6 (III′) Na^+ cations, in general agreement with both experimental structures [1,22]. However, the most significant differences were observed for sites I and I′ occupancies in the theoretical and experimental structures. These differences are attributed to the entropic effects which are beyond the scope of the current approach [17,18]. Four Na^+ cations were located in both sites I and I′ in the primitive unit cell of NaX. Each hexagonal prism (D6R) had two Na^+ cations located in sites I and I′. Site I was displaced some 0.55 Å from the center of D6R along the C_3 axis away from the Na^+ cation in the adjacent site I′. The predicted Na^+–O distances for site I were within 0.3 Å from the experimental values [22]. The Na^+ cation in site I′ was located ca. 1.2 Å above the plane of the 6-ring inside the sodalite cage. The predicted Na^+–O distances for site I′ were within 0.1 Å from those in both experimental structures [1,22]. Na^+ cations in the supercages were again found in the vicinity of site III′ preferentially coordinated to the (AlO_4) tetrahedra some 0.3 Å away from both the experimental sites [1,22]. The cation locations and site occupancies are summarized in Table 1.

3.2. CaX and benzene/CaX system

The structure of $Ca_{48}X$ has been determined recently by Vitale et al. [24], and cation locations were predicted by Gorman et al. [17,18]. Similar to the earlier findings [17,18], Ca^{2+} cations were located in sites I and II only, and the predicted structure had *Fd-3* space group symmetry in agreement with the recent crystal data [24]. Slight cation disorder between sites I and I′ observed experimentally was not reproduced by modeling. The comparison of the theoretical and experimental results is shown in Table 1.

Application of a combined molecular dynamics, Monte Carlo and energy minimization approach allowed us to locate benzene molecules in two sites, (i) coordinated facially to the Ca^{2+} cation in site II at a distance of 2.91 Å and sitting at the sixfold axis (Fig. 3), and (ii) in the supercage in the plane of the puckered 12-membered ring on a threefold axis. The host–guest interaction energies for these sites were −75.3 and −32.5 kJ/mol. Benzene locations and interaction energies in $Ca_{48}X$ system were in good agreement with the experimental results of Vitale et al. [24] on $C_6D_6/Ca_{48}X$ and calculations of Henson et al. [25] on benzene adsorbed in Na faujasites with varying Si/Al ratios.

3.3. Zeolite 3A ($K_{15}Na_9A$)

The structure of the dehydrated zeolite 3A was solved by Adams and Haselden [26]. They found three crystallographic sites for K^+ cations located in the 6-rings, 8-rings and 4-rings, and one site for Na^+ cations in the 6-rings (Fig. 4). The present simulation not only

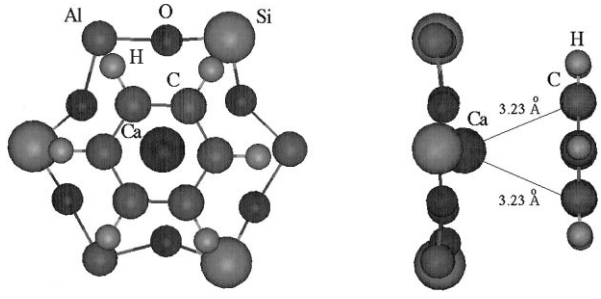

Fig. 3. Location of benzene molecules at Ca^{2+} cation in Site II of CaX (Si/Al=1.0).

Table 1
Experimental [1,22,24] and predicted cation locations and unit cell occupancies in faujasites

Sites	Location	Experiment [22]	Experiment [1]	This study full cell	This study 4×primitive cell	Experiment [24]	This study
(a) $Na_{88}X$							
I	Center of D6R	2.9	0	–	16		
I′	6-Rings of D6R	29.1	32	32 [1]	16		
II	6-Rings of β-cages	31	32	32 [1]	32		
III′	At O4 on 4R edge	10.6	0	–	–		
III′	At Al atom off 4R edge	10.6	24	18	20		
III′	At Si atom off 4R edge	8.6	0	6	4		
(b) $Ca_{48}X$							
I	Center of D6R					11.9	–
I′	6-Rings of D6R					5	16
II	6-Rings of β-cages					31.1	32

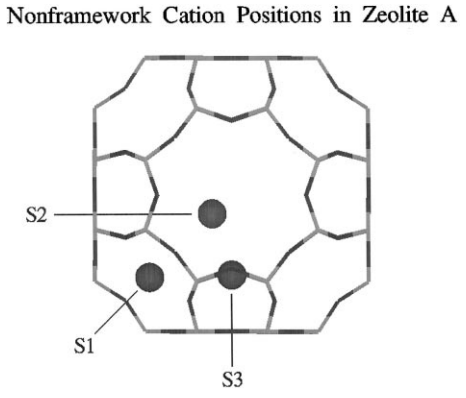

Fig. 4. Non-framework cation positions in zeolite A.

Table 2
Experimental [26] and predicted cation site occupancies in zeolite 3A

Sites [26]	Location	Experiment [26]	This study
K1	6-Rings (6MR)	28.6	27
K2	8-Rings (8MR)	24	24
K3	4-Rings (4MR)	7.4	9
Na1	6-Rings (6MR)	35.4	36

confirmed these locations, but also accurately predicted the cation partial occupancies (Table 2 and Figs. 5–7).

The present study supports the results of Adams and Haselden [26] demonstrating the absence of zero-coordinated K^+ cations in 8-rings [27]. The predicted K–O distances for the 8-ring sites (2.32, 2.42, and 2.61 Å) are in reasonable agreement with the experimental bond distances (2.538, 3.005, and 3.132 Å).

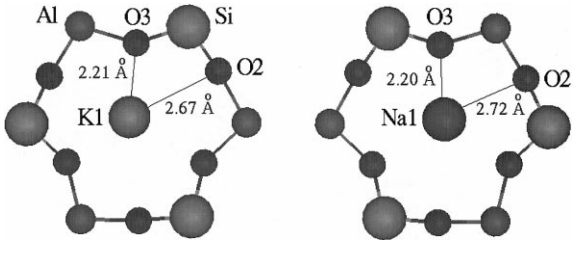

Fig. 5. Predicted K1 and Na1 cation locations in 6MR of zeolite 3A.

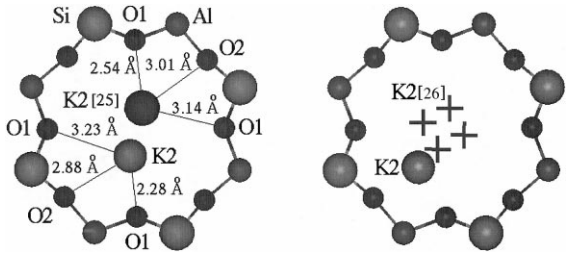

Fig. 6. Predicted K2 and experimental [26] cation locations in 8MR of zeolite 3A.

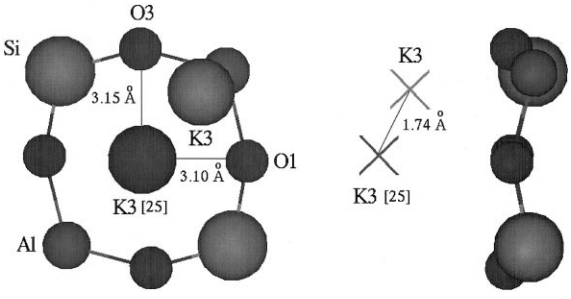

Fig. 7. Predicted K3 and experimental [26] cation locations in 4MR of zeolite 3A.

3.4. Cu-mordenite (Si/Al=5.0)

Cu^{2+} cation were located in Cu-mordenite which contains relatively few non-framework cations due to its high Si/Al ratio. This case is particularly interesting, since the non-framework species in high silica zeolites are difficult to locate by powder diffraction methods.

Cheetham et al. [28] have recently studied Cu^{2+} locations in the hydrated ($Cu_{1.384}T_{48}O_{96}{\cdot}28H_2O$) and partially dehydrated ($Cu_{1.468}T_{48}O_{96}{\cdot}4.04H_2O$) copper-exchanged mordenite. Both structures were refined in the *Cmcm* space group by single crystal X-ray diffraction. Cheetham et al. [28] located three Cu^{2+} sites in the partially dehydrated structure of Cu-mordenite (Fig. 8). Cu(1) site was found to lie in the center of the elliptical 8-ring bound to two O(9) atoms at 2.670 Å and four O(1) atoms at 2.875 Å. Two water molecules, O(1w), at 2.30 Å completed the Cu coordination. Cu(2) site was situated above a 6-ring in the main 12-ring channel. The lowest occupied Cu site, Cu(3), was found to one side of the circular 8-ring that leads to the 12-ring channel. The Cu(3) atoms were

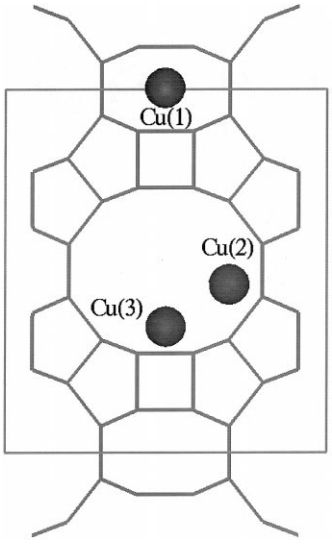

Fig. 8. Cu^{2+} cation locations in partially dehydrated Cu-mordenite viewed along the [0 0 1] direction [28]. Residual water molecules are not shown.

coordinated to two O(2) atoms at 2.68 Å and one O(10) atom at 2.75 Å. The order of site occupancy was found to be Cu(1)>Cu(2)>Cu(3).

The Cu–Oz bond lengths of all three Cu sites are rather long (2.59–2.875 Å), which Cheetham et al. [28] explained by three effects: (i) artificial bond elongation in the X-ray experiment due to low occupancy of the Cu sites, (ii) optimization of the Cu ion position to provide adequate bonding overlap with the Oz atoms, (iii) and the presence of water molecules undetectable by XRD which can stabilize the Cu^{2+} cations and reduce their interaction with the Oz atoms. Tetrahedral aluminum sites in the partially dehydrated sample could not be located due to high apparent framework Si/Al ratio of 25.2.

Since Al atoms could not be located experimentally [28], we first modeled an all-silica mordenite structure in order to compare predicted cation locations with the experimental structural data for Cu-mordenite [28]. The partial charges on the Si atoms were lowered accordingly to yield a uniform charge distribution per T-sites and a total negative charge of −8 per *P1* unit cell of mordenite ($Si_{48}O_{96}$). The four Cu^{2+} ions were then located using the above cation locator procedure. The four Cu^{2+} ions were found to occupy two distinct sites similar to Cu(1) and Cu(3) sites of Cheetham et al. [28]. The predicted Cu(1) site (two Cu^{2+} cations) was located near the center of the elliptical 8-ring bound to two O(12) atoms at 2.73 Å and two O(1) atoms at 2.50 Å. The predicted Cu(1) site (two Cu^{2+} cations) was found to lie ca. 0.55 Å away from the experimental site off the center of the elliptical 8-ring. The Cu^{2+} cations in the Cu(3)-type site were bicoordinated to O(4) and O(13) atoms at 2.15 and 2.37 Å, respectively, in the circular 8-ring that leads to the 12-ring channel. The second Cu^{2+}–O(4) distance was very long, 3.01 Å.

The Cu^{2+} cations in the Si/Al=5.0 unit cell of Cu-mordenite were located in the Cu(3)-type site some 2.20–2.32 Å away from the nearest oxygen atoms (three Cu^{2+} cations). The remaining Cu^{2+} cation was found in the Cu(2)-type site of Cheetham et al. [28] slightly above the plane of the 6-rings in the 12-ring pore channels. In the latter case, the Cu–O distances also indicated strong coordination of Cu ions to framework oxygen anions (2.18–2.60 Å) and the absence of zero-coordinated non-framework species.

We offer two possible explanations for the observed differences between the experimental and predicted cation locations. On the one hand, the Cu^{2+} cations may be stabilized in certain crystallographic sites, e.g. Cu(2) site, by the residual water invisible to the X-rays in the experimental partially hydrated sample. On the other hand, the aluminum distribution in high silica mordenite framework (Si/Al>5.0) may be non-random contrary to our assumption. The cation location pattern will then be affected by how eight Al atoms are distributed among the framework sites. However, the present theory correctly predicted the existence and locations of the three experimental cation sites in Cu-mordenite despite the compositional and structural uncertainties in this system.

The new molecular modeling method located Cu^{2+} ions in three crystallographic sites similar to experimental Cu(1), Cu(2) and Cu(3) sites recently found by Cheetham et al. [28]. The Cu(2) and Cu(3) sites located in the main 12-ring channels or 8-rings that form part of the wall of the 12-ring channels are highly accessible to the gas phase NO and ammonia molecules passing through the zeolite pore structure. On the other hand, the low coordination of the Cu^{2+} cations in Cu(2) and Cu(3) sites makes them available for interaction with NO, and therefore, more susceptible to

deNO$_x$ catalysis [29]. The Cu(1) site located in the elliptical 8-ring is less accessible to gas molecules. This site is unlikely to play a significant role in deNO$_x$ chemistry.

Therefore, high accessibility and low coordination of Cu^{2+} ions provide a possible explanation for the high activity of Cu-mordenite system in deNO$_x$ catalysis [28]. By comparison, Cu-exchanged zeolites X and Y are relatively inactive in the deNO$_x$ catalysis. This is in line with the observation that the majority of Cu^{2+} cations in zeolites X and Y are located inside the sodalite cages or hexagonal prisms where they are highly coordinated to the framework oxygen atoms and inaccessible to gas phase molecules [30].

4. Conclusions

The present study demonstrated the potential of the new grid-based and structure optimization approaches to predict locations of various non-framework species in zeolites. In the case of charge-balancing cations, not only their locations, but also the partial occupancies may be determined. Moreover, the combination of the new approach with traditional Monte Carlo and energy minimization techniques allows to accurately locate other non-framework species, such as benzene molecules. In many cases, where solving crystal structures of zeolites with known framework types from powder diffraction data is a challenge, the new method can provide a realistic initial structural model for locations of the non-framework species.

Acknowledgements

VVG wishes to thank F. Notaro and Praxair Inc. for support and encouragement during the preparation of this paper.

References

[1] G. Vitale, C.F. Mellot, L.M. Bull, A.K. Cheetham, J. Phys. Chem. B 101 (1997) 4559.
[2] J. Plévert, F. Di Renzo, F. Fajula, G. Chiari, J. Phys. Chem. B 101 (1997) 10340.
[3] J.J. Van Dun, W.J. Mortier, J. Phys. Chem. 92 (1988) 6740.
[4] J.J. Van Dun, K. Dhaeze, W.J. Mortier, J. Phys. Chem. 92 (1988) 6747.
[5] J.J. Van Dun, K. Dhaeze, W.J. Mortier, D.E.W. Vaughan, J. Phys. Chem. Solids 50 (1989) 469.
[6] E. Smolders, J.J. Van Dun, W.J. Mortier, J. Phys. Chem. 95 (1991) 9908.
[7] J.L. Lievens, W.J. Mortier, K.-J. Chao, J. Phys. Chem. Solids 53 (1992) 1163.
[8] J.L. Lievens, W.J. Mortier, J.P. Verduijn, J. Phys. Chem. 96 (1992) 5473.
[9] J.L. Lievens, J.P. Verduijn, A.-J. Bons, W.J. Mortier, Zeolites 12 (1992) 698.
[10] J.L. Lievens, J.P. Verduijn, W.J. Mortier, Zeolites 12 (1992) 690.
[11] W.J. Mortier, D.E.W. Vaughan, J.M. Newsam, in: W.H. Flank, T.E. Whyte (Eds.), Perspectives in Molecular Sieve Science, ACS Symposium Series, vol. 368, American Chemical Society, Washington, DC, 1988, p. 194.
[12] J.M. Newsam, C.M. Freeman, A.M. Gorman, B. Vessal, J. Chem. Soc., Chem. Commun. (1996) 1945.
[13] M.E. Grillo, J. Carrazza, J. Phys. Chem. 100 (1996) 30.
[14] D.H. Olson, J. Phys. Chem. 74 (1970) 2758.
[15] V. Gramlich, W.M. Meier, Z. Kristallogr. Kristallgeom. Kristallphys. Krystallchem. 133 (1971) 134.
[16] A. Alberti, P. Davoli, G. Vezzalini, Z. Kristallogr. 175 (1986) 249.
[17] A.M. Gorman, C.M. Freeman, C.M. Koelmel, J.M. Newsam, Faraday Discuss. 106 (1997) 489.
[18] C.M. Freeman, Faraday Discuss. 106 (1997) 506.
[19] InsightII 4.0.0 program, Molecular Simulations Inc., San Diego, 1996.
[20] Discover 3.2, forcefield simulations program, Molecular Simulations Inc., San Diego, 1996.
[21] Catalysis 4.0.0 programs, Molecular Simulations Inc., San Diego, 1996.
[22] D.H. Olson, Zeolites 15 (1995) 439.
[23] Yu.I. Smolin, Yu.F. Shepelev, I.K. Butikova, V.P. Petranovskii, Sov. Phys. Crystallogr. 28 (1983) 36.
[24] G. Vitale, L.M. Bull, R.E. Morris, A.K. Cheetham, B.H. Toby, C.G. Coe, J.E. MacDougall, J. Phys. Chem. 99 (1995) 16087.
[25] N.J. Henson, A.K. Cheetham, A. Redondo, S.M. Levine, J.M. Newsam, Zeolites and Related Materials: State of the Art 1994, Stud. Surf. Sci. Catal. 84 (1994).
[26] J.M. Adams, D.A. Haselden, J. Solid State Chem. 47 (1983) 123.
[27] P.C.W. Leung, M.B. Kunz, K. Seff, I.E. Maxwell, J. Phys. Chem. 79 (1975) 2157.
[28] M.P. Attfield, S.J. Weigel, A.K. Cheetham, J. Catal. 170 (1997) 227.
[29] I.E. Wachs, G. Deo, M. de Boer, J. Catal. 160 (1996) 322.
[30] I.E. Maxwell, J.J. de Boer, J. Phys. Chem. 79 (1975) 1875.